Journal of Research and Applications in Mechanical Engineering
ISSN: 2229-2152 (Print); 2697-424x (Online)
(2024) Vol. 12, No. 2, Paper No. JRAME-24-12-018
[DOI: 10.14456/jrame.2024.18]

Research Article

Nonlinear Analysis of New Electromagnetic Vibration Actuator

H. Yaguchi*
R. Sato
Faculty of Engineering, Tohoku Gakuin University, Sendai, Miyagi, 984-8588, Japan

Received 26 September 2023
Revised 30 November 2023
Accepted 8 December 2023

Abstract:
The inspection and maintenance of infrastructure such as bridges, which may collapse during an earthquake, is important. Numerous robots have been proposed for structural inspections. These robots have complicated mechanisms and require the adhered device to have a relatively large weight. The authors previously proposed an electromagnetic vibration actuator for structural inspection. However, an analysis that considers the nonlinearity of the translational spring was not performed for this actuator. In this study, a dynamic analysis that considers the nonlinearity of the vibration component is performed. Furthermore, a prototype of the vibration actuator is constructed and its movement characteristics are measured. The measurement and theoretical analysis results are in relatively good agreement, verifying the validity of the theoretical analysis. Based on the theoretical analysis, the movement characteristics of the vibration actuator can be calculated for various parameter values. This paper demonstrates the possibility of applying the theoretical analysis to calculations for other highly nonlinear models in which the electromagnetic force and vibration systems are combined.

Keywords: *Actuator, Vibration, Nonlinear dynamics*

1. Introduction

The aging of large steel structures such as bridges has become a problem. Old bridges may collapse due to the lack of seismic standards when they were built. Furthermore, many bridges require vehicle weight limits due to damage and deterioration caused by aging. The inspection and maintenance of infrastructure such as bridges is thus important. However, bridge inspection is very difficult. Many inspection robots, such as electromagnetic type [1], crawler type [2] and magnetic wheel type [3, 4], have been proposed. These robots use an electromagnetic motor as a drive source and require a large number of reducers and additional devices between the motor and the mechanical part. The movement characteristics of robots based on electromagnetic motors is not expected to improve. Many flying-type robots, such as drones [5, 6], have been proposed. However, these robots require a skilled operator and are affected by weather.

A vibration actuator capable of movement on a magnetic material in which an electromagnetic force and mechanical resonance are coupled was previously proposed by the authors [7, 8]. This vibration actuator has a simple structure and can be inexpensively manufactured. To make this vibration actuator lightweight and compact, an electromagnet is inserted into the vibration component. This vibration component thus exhibits the nonlinear behavior of a soft spring. However, an analysis that considers the nonlinearity of the translational spring has not been performed for this actuator.

* Corresponding author: H. Yaguchi
E-mail address: yaguchi@mail.tohoku-gakuin.ac.jp

In this study, a dynamic analysis that considers the nonlinearity of the vibration component is performed. In the analysis, the vibration component is replaced by a one-degree-of-freedom model with viscous damping. The translational spring with the nonlinear behavior of a soft spring is replaced with an equivalent linear spring constant. A theoretical analysis is performed for the case where the force-displacement characteristics of the translational spring are asymmetrical with respect to the origin. The frequency response of the vibration actuator is calculated. In addition, a static analysis of the movement of the vibration actuator is carried out. This paper shows that the movement characteristics of the vibration actuator can be calculated using a theoretical analysis by combining dynamic and static analyses. Furthermore, a prototype of the vibration actuator is constructed and its movement characteristics are measured. For this vibration actuator, it is shown that the driving method using the nonlinearity of the translational spring can greatly improve the movement characteristics compared to those in the linear case. The measurement and theoretical analysis results are in relatively good agreement, verifying the validity of the theoretical analysis. Therefore, the movement characteristics of the vibration actuator can be calculated for various parameter values. Finally, design guidelines for engineering actuators are established.

2. Vibration Component with Nonlinear Restoring Force

Fig. 1 shows the vibration actuator capable of movement on a magnetic material. The vibration actuator consists of a vibration component, a triangular acrylic frame, a permanent magnet, and natural rubber (the latter two items are attached to the bottom of the triangular acrylic frame). The permanent magnet is used for holding the actuator on a magnetic material. The magnet has a diameter of 10 mm and a thickness of 4 mm. Natural rubber with a thickness of 1 mm is attached to the lower part of the permanent magnet to increase the frictional force. The vibration component consists of a cylindrical permanent magnet, a translational spring, and an electromagnet. The translational spring is made of stainless steel and has an outer diameter of 12 mm, a free length of 25 mm, and a spring constant k.

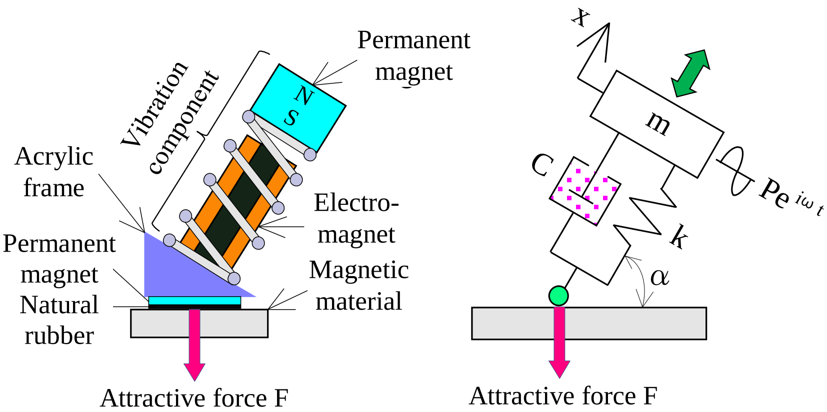

(a) Structure of vibration actuator

(b) Photograph of vibration actuator

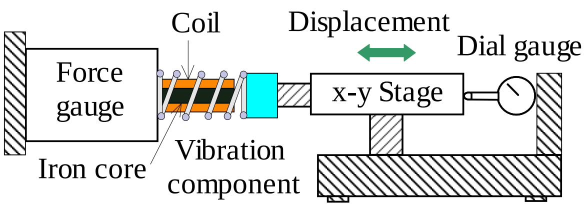

(c) Apparatus for force-displacement measurements

Fig. 1. Schematic diagram of vibration actuator and apparatus for force-displacement measurements.

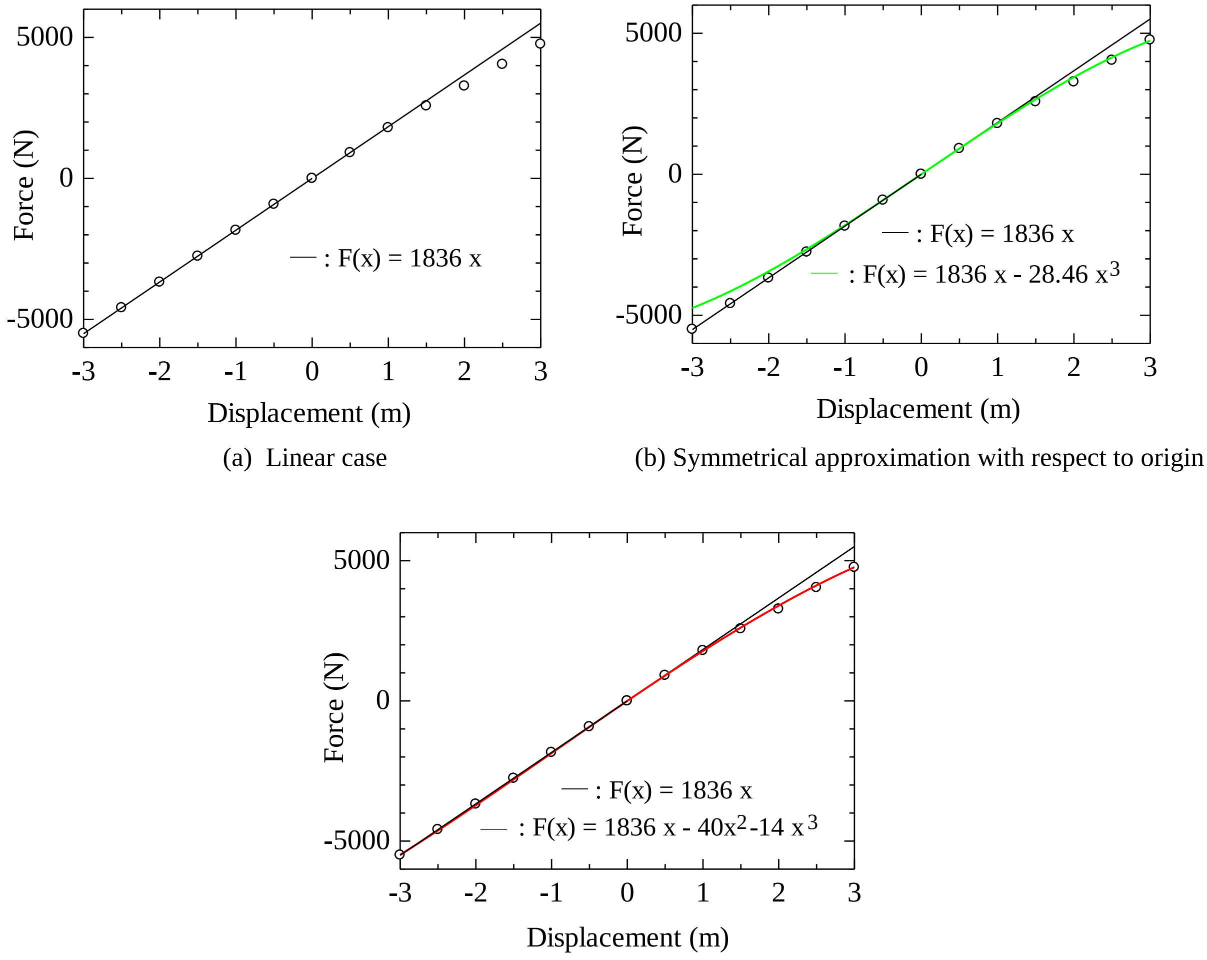

(a) Linear case

(b) Symmetrical approximation with respect to origin

(c) Asymmetrical approximation with respect to origin

Fig. 2. Translational spring with nonlinearity.

The permanent magnet is a cylindrical NdFeB magnet magnetized in the axial direction. It has a diameter of 12 mm, a height of 5 mm, and a mass m of 1.85 g. An electromagnet with an iron core (diameter: 3.5 mm, length: 22 mm) with 840 turns of 0.2-mm copper wire was used in the experiment. The electromagnet was inserted into the translational spring. The angle α of the vibration component was set to 60° based on results obtained in a previous study [7]. The electromagnetic excitation force due to attraction and repulsion during one period of vibration acts on the permanent magnet. The vibration actuator has a height of 40 mm, a width of 15 mm, and a total mass M_a of 19.3 g.

To design a compact vibration actuator, the electromagnet was inserted into the translational spring of the vibration component. In such a magnetic circuit, due to the influence of the attractive force between the permanent magnet and the iron core within the electromagnet, the translational spring behaves as a soft spring. The vibration component of the actuator is the electromagnet inserted into the translational spring. Due to the influence of the attractive force between the permanent magnet and the iron core within the electromagnet, the translational spring behaves as a soft spring. In order to measure the force-displacement relationship for the translational spring, a measuring device that includes a force gauge and an *x*-*y* stage was used, as shown in Fig. 1(c). For the translational spring into which the electromagnet is inserted, the displacement relationship was measured when compressive and tensile forces were applied to the spring. In the figures, a positive sign indicates compression and a negative sign indicates tensile displacement. In the measurements, the translational spring was displaced from -3 mm to 3 mm. The results converted into SI units are shown in Figs. 2(a) to 2(c) using ○ marks. The linear approximation of the plotted points is indicated by black lines. A spring constant k = 1836 N/m was used for the translational spring in the linear approximation.

The relationship between force and displacement approximated using the following equation is shown by the green line in Fig. 2(b).

$$F(x) = k\,x - \mu\,x^3 = 1836\ x - 28.46\,x^3 \tag{1}$$

When approximated by equation (1), the relationship between force and displacement is symmetrical with respect to the origin and the nonlinearity of the translational spring cannot be accurately expressed. The result of approximating the nonlinearity of the translational spring by the following equation is shown by the red line in Fig. 2(c).

$$F(x) = k\,x - \lambda\,x^2 - \mu\,x^3 = 1836\,x - 40\,x^2 - 14\,x^3 \tag{2}$$

With equation (2), the nonlinearity of the translational spring with asymmetry with respect to the origin can be almost exactly approximated.

3. Dynamic Analysis of Vibration Actuator Considering Nonlinearity

In this paper, a dynamic analysis that considers the nonlinearity of the translational spring is conducted. The effect of the spring in the natural rubber attached to the bottom of the actuator is ignored and the vibration component is replaced by the one-degree-of-freedom model with viscous damping. The mass of the permanent magnet in the vibration component is *m*, the spring constant for the translational spring material is *k*, the viscous damping coefficient is *C*, and the displacement coordinate of the mass m is *x*. It is assumed that the restoring force *F(x)* produced by the translational spring is defined by the nonlinear restoring force given in equation (2). Mass *m* is considered to vibrate under a harmonic excitation force $Pe^{i\omega t}$, where *P* is the force amplitude, ω is the angular frequency, and *t* is time. For the displacement *x* of mass *m*, let *A* be the vibration amplitude and φ be the phase.

$$x = A\cos\theta,\ \theta = \omega\,t - \varphi \tag{3}$$

In the above equation, the nonlinear restoring force *F(x)* with respect to the displacement *x* is represented by a Fourier series. Assuming that the displacement of mass *m* varies at the same frequency as the excitation force, the following equation is obtained with *D* as a coefficient.

$$\left.\begin{aligned} F_2(x) &= kx - \lambda x^2 - \mu x^3 \\ &= k\,A\cos\theta - \lambda\,A^2\cos\theta - \mu\,A^3\cos^3\theta \\ &= D\cos\theta \end{aligned}\right\} \tag{4}$$

The coefficient *D* is calculated in the same way that the coefficients of the Fourier series are found.

$$\left.\begin{aligned} D &= \frac{1}{\pi}\int_0^{2\pi}(k\,A\cos\theta - \lambda\,A^2\cos^2\theta - \mu\,A^3\cos^3\theta)\ \ \cos\theta\,d\theta \\ &= k\,A - \frac{3}{4}\mu\,A^3 \end{aligned}\right\} \tag{5}$$

The following equation is obtained from the restoring force $F(x) = D\cos\theta$.

$$F(x) = D\frac{x}{A} = \left(k\,A - \frac{3}{4}\mu\,A^3\right)\frac{x}{A} = k^*x \tag{6}$$

where

$$k^* = k\ \left(1 - \frac{3}{4}\varepsilon\,A^2\right),\ \varepsilon = \frac{\mu}{k} \tag{7}$$

k^* in the above equation is the equivalent linear spring constant. In the above calculation, the x^2 term vanishes, so the equivalent linear spring constant is used for this squared term. Expressing the nonlinearity by a quadratic equation, the restoring force *F(x)* is given as follows [9].

$$F(x) = k\,x - \lambda\,x^2 = \left(k\sqrt{1 + 2\,\sigma^2 A^2}\right)\,x, \sigma = \frac{\lambda}{k} \tag{8}$$

Combining the third-order nonlinear term in equations (7) and (8) yields the following equation of motion for the one-degree-of-freedom model with *i* as the imaginary unit.

$$m\frac{d^2x}{dt^2} + k\left(\sqrt{1 + 2\,\sigma^2 A^2} - \frac{3}{4}\varepsilon\,A^2\right)\,x + C\frac{dx}{dt} = Pe^{i\omega t} \tag{9}$$

Let A be the vibration amplitude of mass m and assume that the general solution of equation (9) is as follows.

$$x = A\,e^{i\omega t} \tag{10}$$

Substituting equation (10) into equation (9) yields the following equation.

$$\left(p^2\delta - \omega^2 + i\,\frac{\omega\,C}{m}\right)\,A = q \tag{11}$$

where

$$p = \sqrt{\frac{k}{m}}, q = \frac{P}{m}, \delta_{st} = \frac{P}{k}, \delta = \sqrt{1 + 2\,\sigma^2 A^2} - \frac{3}{4}\varepsilon\,A^2 \tag{12}$$

In addition, the following quantities and dimensionless quantities are introduced.

$$\bar{\omega} = \frac{\omega}{p}, \bar{\sigma} = \sigma\,\delta_{st}\,, \bar{\varepsilon} = \varepsilon\,\delta_{st}^2\,, \varsigma = \frac{C}{2\sqrt{mK}}\;\;, \bar{\delta} = \sqrt{1 + 2\,\bar{\sigma}^2\bar{A}^2} - \frac{3}{4}\bar{\varepsilon}\,\bar{A}^2 \tag{13}$$

When equation (13) is introduced, the vibration amplitude A of mass m is expressed as follows from equation (11).

$$A = A_a e^{i\,\varphi}\,, A_a = \frac{\delta_{st}}{\sqrt{(\bar{\delta} - \bar{\omega}^2)^2 + (2\,\varsigma\,\bar{\omega})^2}}\;, \tan\varphi = \frac{2\,\varsigma\bar{\omega}}{\bar{\delta} - \bar{\omega}^2} \tag{14}$$

Since A_a in the formula is the actual vibration amplitude of mass m, A is replaced with A_a, as shown in the following equation.

$$\bar{A}_a = \bar{A} = \frac{A_a}{\delta_{st}} \tag{15}$$

Expanding equation (15) yields the following 12th-order equation for the dimensionless vibration amplitude.

$$\eta_1\bar{A}^{12}{}_a + \eta_2\bar{A}^{10}{}_a + \eta_3\bar{A}^{8}{}_a + \eta_4\bar{A}^{6}{}_a + \eta_5\bar{A}^{4}{}_a + \eta_6\bar{A}^{2}{}_a - 1 = 0 \tag{16}$$

Where

$$\left.\begin{aligned}
&\eta_1 = -\left(\frac{9}{16}\,\bar{\varepsilon}^2\right)^2, \;\; \eta_2 = \frac{9}{2}\bar{\sigma}^2\bar{\varepsilon}^2 - \frac{9}{8}\bar{\varepsilon}^2\left(\frac{3}{2}\;\bar{\varepsilon}\,\bar{\omega}^2 + 2\,\bar{\sigma}^2\right)\\
&\eta_3 = 12\;\bar{\sigma}^2\bar{\varepsilon}\,\bar{\omega}^{\,2} - \left(\frac{3}{2}\;\bar{\varepsilon}\,\bar{\omega}^2 + 2\,\bar{\sigma}^2\right)^2 - \frac{9}{8}\,\bar{\varepsilon}^2\,(1 + \bar{\omega}^4 + 4\,\varsigma^2\bar{\omega}^2)\\
&\eta_4 = 6\;\bar{\varepsilon}\,\bar{\omega}^2 + 8\,\bar{\sigma}^2\bar{\omega}^4 - \frac{9}{8}\;\bar{\varepsilon}^2 - \;(3\;\bar{\varepsilon}\;\bar{\omega}^2 + 4\;\bar{\sigma}^2)\;(1 + \bar{\omega}^4 + 4\,\varsigma^2\bar{\omega}^2)\\
&\eta_5 = (3\;\bar{\varepsilon}\;\bar{\omega}^2 + 4\,\bar{\sigma}^2) - (1 + \bar{\omega}^4 + 4\,\varsigma^2\bar{\omega}^2)^2 + 4\,\bar{\omega}^4\,, \;\; \eta_6 = 2\;(1 + \bar{\omega}^4 + 4\,\varsigma^2\bar{\omega}^2)^2
\end{aligned}\right\} \tag{17}$$

A program in the MATLAB language was developed to calculate the dimensionless vibration amplitude in equation (16). If the nonlinear terms shown in equations (7) and (8) are set to $\sigma = \varepsilon = 0$, the vibration amplitude of the one-degree-of-freedom model in the linear state can be obtained.

4. Static Analysis of Vibration Actuator

As shown in Fig. 3, for this vibration actuator, the vibration component can vibrate by being held by the attraction force of the permanent magnet in the support. The vertical and horizontal force components generated by the vibration component periodically change the holding force of the support. When the horizontal component force exceeds the frictional force, the vibration actuator can move in one direction. In order to clarify this operating principle, the authors previously conducted a theoretical analysis of the movement of vibration actuators, to which the energy method was applied [7]. However, this analysis did not take into account the load mass mounted on the actuator and the traction force, so the propulsion characteristics of the actuator could not be estimated. Therefore, in this paper, a static analysis that considers their influence is performed. As shown in Fig. 3, the amplitude and force generated by the vibration component are denoted as A_a and F_a, respectively. For this vibration actuator, it is assumed that the vibration displacement A_a is movement while maintaining a steady state. Now, let us consider the state in which the actuator is held by the attractive force F of the permanent magnet on a slope made of a magnetic material with angle β. Let M be the load mass mounted on the actuator, g be the gravitational acceleration, W be the traction force, and μ be the coefficient of friction between the magnetic material and the natural rubber. When the mass m of the vibration component is displaced in the positive x direction, as shown in Fig. 3(a), the following equation is obtained from the balance between the frictional force F_f when the actuator moves along a slope (climbing) and the force when the actuator starts to slide forward.

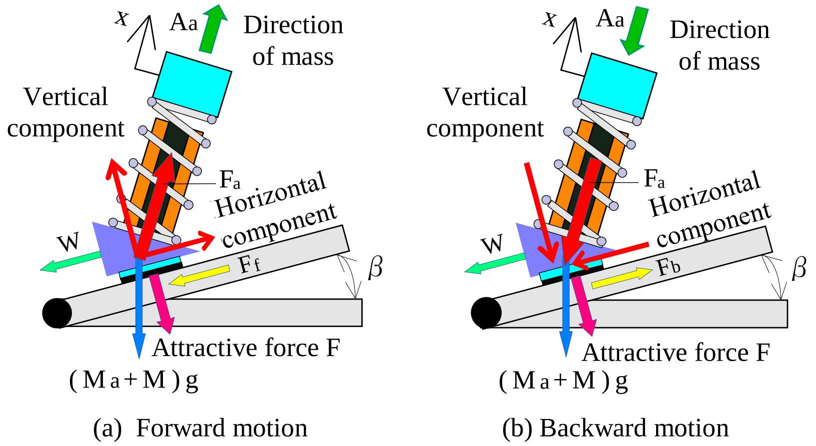

Fig. 3. Vibration actuator moving on slope made of magnetic material.

$$F_f = \mu \{ F - F_a \sin\alpha + (m + M) \ g\cos \beta \}, F_a \cos \alpha = F_f + (m + M) \ g\sin\beta + W \tag{18}$$

Conversely, when the mass m is displaced in the negative x direction, as shown in Fig. 3(b), the following equation is obtained from the balance between the frictional force F_b when the vibration actuator retreats along the slope (downhill) and the force when it starts to slide backwards.

$$F_b = \mu \{ F + F_a \sin \alpha + (m + M) \ g\cos \beta \}, F_a \cos\alpha = F_b - (m + M) \ g\sin\beta - W \tag{19}$$

Assuming that the vibration component is harmonically vibrating, the maximum value of the kinetic energy T of the mass m and the elastic energy U due to the spring constant k are equal according to the law of conservation of energy. Considering this, the elastic energy U (= kinetic energy T) generated by the vibration component is equal to the energy dissipated by friction and the work done by gravity. In addition, as $F_a = k\, A_a$ in the above equations, the following quantities and dimensionless quantities are introduced.

$$\bar{F}_a = \frac{F_a}{F}, \quad \bar{m}_a = \frac{m_a g}{F}, \bar{M} = \frac{M g}{F}, \bar{W} = \frac{W}{F}, \bar{U} = \frac{U}{F}, U = \frac{1}{2} k \, {A_a}^2 \left(= \ \frac{1}{2} m \ \left(\frac{dA_a}{dt}\right)^2 \right) \tag{20}$$

The forward and backward displacements δ_f and δ_b, respectively, during one cycle of vibration are expressed as follows.

$$\left.\begin{aligned}\delta_f &= \frac{\bar{U}\cos\alpha}{\{\mu-\mu\bar{F}_a\sin\alpha+\mu(\bar{M}_a+\bar{M})\cos\beta+(\bar{M}_a+\bar{M})\sin\beta+\bar{W}\}}\\ \delta_b &= \frac{\bar{U}\cos\alpha}{\{\mu+\mu\bar{F}_a\sin\alpha+\mu(\bar{M}_a+\bar{M})\cos\beta-(\bar{M}_a+\bar{M})\sin\beta-\bar{W}\}}\end{aligned}\right\} \tag{21}$$

If the driving frequency of the vibration actuator is f (Hz), the real forward displacement δ of the actuator is regarded as the difference between the forward and backward displacements.

$$\delta = f\,(\delta_f - \delta_b) \tag{22}$$

5. Specifications of Vibration Components and Force Generated by Electromagnets

The damping ratio $\zeta = 0.0195$ for the translational spring was measured from the damped free vibration curve obtained by applying an initial displacement to the vibration component with the electromagnet inserted. For the translational springs, the nonlinear coefficients for the curve fitting that included the cubic term in equation (1) are $\sigma = 0$ and $\varepsilon = 0.0155$ from equation (7). The nonlinear coefficients for the curve fitting that included the second- and third-order terms are $\sigma = 0.021786$ and $\varepsilon = 0.0076253$ from equation (8). Combining the above nonlinear terms, σ and ε, the vibration amplitudes when the nonlinearity is symmetrical and asymmetrical with respect to the origin can be calculated from equation (16).

Using the experimental apparatus shown in Fig. 1(c), the relationship between the input current to the electromagnet inserted in the vibration component and the force generated in the permanent magnet was measured. In the measurement, the attractive and repulsive forces generated in the permanent magnet were measured by changing the input current to the electromagnet. Table 1 shows the relationship between the input current and the average attractive and repulsive forces. These results were obtained with a direct current passed through the electromagnet. In the measurement of the movement of the vibration actuator, described later, the effective value of the alternating current input to the electromagnet was measured with a power analyzer. Considering this, the value of the force amplitude P of the forced excitation force shown in equation (9) was calculated as 1.41 times the effective value. From this, the δst in equation (12) required for the theoretical analysis was calculated as shown in Table 1.

Table 1: Relationship between input current to electromagnet and excitation force.

Current (A)	**Effective force amplitude (N)**	**Maximum force amplitude (N)**	**δ_{st} (mm)**
0.0125	0.0152	0.0215	0.0117
0.025	0.0298	0.0421	0.0229
0.0375	0.0445	0.0629	0.0343
0.05	0.0592	0.0837	0.0456
0.0625	0.0738	0.1044	0.0569
0.075	0.0881	0.1246	0.0679
0.0875	0.1032	0.1459	0.0795
0.1	0.1178	0.1666	0.0907

6. Frequency Response and Locomotion Characteristics of Vibration Actuator

An experimental test was conducted using the apparatus shown in Fig. 4. As the magnetic material, an iron rail with a width of 50 mm, a thickness of 50 mm, and a length of 500 mm was used.

The vibration actuator was placed on the iron rail. The vibration component was driven using a function generator and an amplifier. The resonance frequency at the small amplitude of the vibration component was 104 Hz (linear case). The input current and power to the electromagnets in the vibration component were measured using a power analyzer. The coefficient of friction μ between the iron rail and the natural rubber measured in the experiment was 0.97. The attractive force F of the permanent magnet attached to the bottom of the frame was 4.6 N, as measured using a force gauge.

The frequency dependence on the vibration amplitude and speed of the vibration actuator with the inserted vibration component was investigated. Fig. 5(a) shows the relationship between the vibration frequency ratio F_r normalized by the resonance frequency of 104 Hz (linear case) when the vibration component has a minute amplitude and the vibration amplitude A_a of the vibration component while the vibration actuator is moving in the horizontal plane. As shown in Fig. 4, the vibration amplitude A_a was measured using a high-speed data logger with a laser displacement meter placed at a moving point of the vibration actuator. The movement speed was measured at the same time.

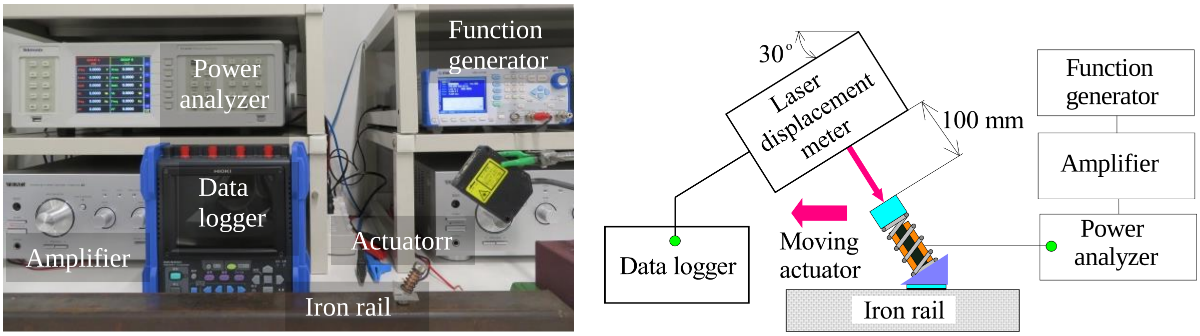

Fig. 4. Experimental apparatus for examining movement characteristics of vibration actuator.

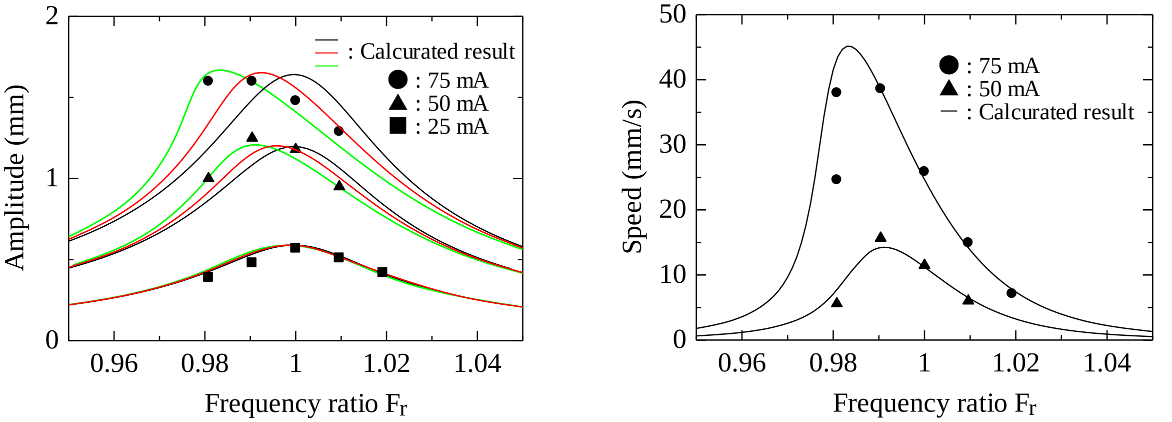

(a) Frequency response of vibration component

(b) Speed of vibration actuator

Fig. 5. Frequency response of vibration component and speed of vibration actuator.

The measurement results when an input current (rms value) of 50 or 75 mA is applied to the electromagnet are shown in the figure using ▲ and ● marks, respectively. When the attractive force F is as high as 4.6 N, as in this actuator, the vibration amplitude when the vibration component is fixed is equal to that when the actuator is moving. The actuator could not move when a current of 25 mA was applied to the electromagnet; the results when the actuator was fixed are shown using the ■ mark. From the figure, as the input current to the electromagnet increases, the nonlinear effect in the translational spring becomes more pronounced. The black line is the theoretical analysis result calculated from equation (16) with the nonlinear coefficient $\sigma = \varepsilon = 0$ (linear case). The red line is the result obtained with $\sigma = 0.021786$ and $\varepsilon = 0.0076253$ (considering the second- and third-order terms) and the green line is the result obtained with $\sigma = 0$ and $\varepsilon = 0.0155$ (considering only the third-order term) to approximate the nonlinearity of the translational spring. The measurement results are asymptotic to the theoretical analysis results obtained considering only the third-order term. This is because the nonlinearity of the translational spring is relatively weak in this actuator, and thus the vibration components are almost harmonically vibrating, eliminating the influence of the second harmonic. For a strong magnetic circuit with pronounced nonlinearity of the vibration component, the nonlinearity of the translational spring is prominent. For this reason, the analytical method presented in this paper is considered to provide effective solutions for models with stronger nonlinearity. In the following, the nonlinearity of the spring is calculated using parameters ($\sigma = 0$, $\varepsilon = 0.0155$) that consider only the third-order nonlinear term.

Fig. 5(b) shows the relationship between the frequency ratio F_r and the movement speed of the vibration actuator in the horizontal plane. The solid line is the theoretical result calculated using equation (22) with the inclination angle β of the iron rail set to 0. The theoretical results and the measurement results are in general agreement. When the frequency ratio F_r is 0.98 or 0.99, the movement speed is greatly increased compared to that for the linear case (F_r = 1). Therefore, for an actuator in which vibration and electromagnetic force are combined, it is possible to greatly improve the movement characteristics by considering the nonlinearity of the translational spring.

Fig. 6 shows the relationship between the load mass M_w attached to the vibration actuator and the vertical upward speed, with the input current (rms value) to the electromagnet of the vibration component fixed at 50 or 75 mA. The load mass was attached with strings to the acrylic frame of the actuator. In the figure, ○, ● and △, ▲ marks are the measurement results when the driving frequency ratio of the actuator is F_r = 0.99 (103 Hz, Case of nonlinear) and F_r = 1 (104 Hz, Case of linear), respectively. The solid line is the theoretical result calculated using equation (22) with the tilt angle β of the iron rail set to 90° and W (as $W = M_w g$) in equation (20) varied. In the figure, the linear and nonlinear results are distinguished using arrows. The figure shows that by considering the nonlinearity of the spring and shifting the resonance point in the linear state by 1 Hz, the propulsion characteristics in the linear state are greatly improved. The actuator can move vertically at a speed of 2.7 mm/s while pulling an additional mass of 120 g. The plot points are along the solid line, verifying the validity of the theoretical analysis.

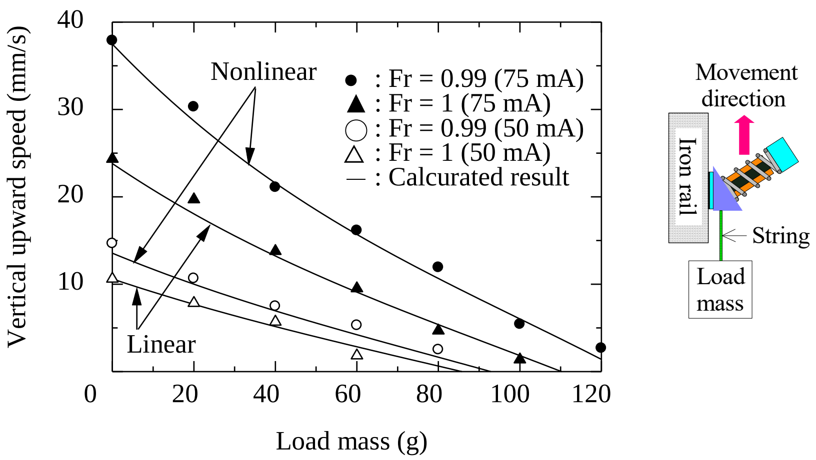

Fig. 6. Relationship between load mass and vertical upward speed.

7. Conclusion

In this study, a dynamic analysis that considered the nonlinearity of the soft spring in a vibration component and a static analysis of the movement in a vibration actuator were performed. In addition, a prototype of the vibration actuator was constructed and its movement characteristics were measured. The theoretical analysis results generally agreed with the measurement results, verifying the validity of the theoretical analysis. It was shown that the vibration actuator can move vertically while pulling a load mass of 120 g, which is about 6.2 times its own weight, by a driving method that utilizes the nonlinearity of a translational spring. The operation of a vibration actuator that is lightweight, compact, and easily driveable was established.

Based on the theoretical analysis presented in this paper, the movement characteristics of the vibration actuator can be calculated for various parameter values. Furthermore, the theoretical analysis can be applied to calculations of other highly nonlinear models in which electromagnetic force and vibration systems are combined.

However, since the size of this actuator is very small, it cannot be applied to inspecting structures at this stage. In general, the electromagnetic force for the excitation source of this actuator is proportional to the cube of the volume. By doubling or tripling the volumes of the permanent magnets and electromagnets of the actuator in this paper, a dramatic improvement in propulsion characteristics is expected. Furthermore, in order to improve propulsion characteristics, we plan to develop a measurement system for bridge inspection that uses a group configuration of actuators.

The actuator proposed in this paper is a linear motor that can be driven directly without the need for additional equipment. Since this actuator is lightweight and controllable, it has the potential to propose a new driving source for robots through future development.

Acknowledgment

This work was supported by JSPS KAKENHI Grant Number JP23K03648.

References

[1] Suzuki M, Hirose S. Proposal of swarm type wall climbing robot system anchor climber and development of adhering mobile units. Journal of the Robotics Society of Japan. 2010;28(5):614-623. (In Japanese)

[2] Shen W, Gu J, Shen Y. Permanent magnetic system design for the wall-climbing robot. IEEE International Conference Mechatronics and Automation; 2005 Jul 29 - Aug 1; Niagara Falls, Canada. USA: IEEE; 2005. p. 2078-2083.

[3] Qin W, Bird JZ. Electrodynamic wheel magnetic rolling resistance. IEEE Trans Magn. 2017;53(8):1-7.

[4] Khirade NR, Sanghi RK, Tidke DJ. Magnetic wall climbing devices - a review. IOSR J Mech Civ Eng. 2014;11(ICAET-2014):55-59.

[5] Mahamud N, Shahriar GM, Khan HU, Sharmin S, Lisa NJ. ALW drone: A new design and efficient approach. 19th International Conference on Computer and Information Technology (ICCIT); 2016 Dec 18-20; Dhaka, Bangladesh. USA: IEEE; 2017. p. 474-479.

[6] Morita M, Kinjo H, Sato S, Sulyon T, Anezaki T. Autonomous flight drone for infrastructure (transmission line) inspection (3). International Conference on Intelligent Informatics and Biomedical Sciences (ICIIBMS); 2017 Nov 24-26; Okinawa, Japan. USA: IEEE; 2018. p. 198-201.

[7] Yaguchi H, Sakuma S. Vibration actuator capable of movement on magnetic substance based on new motion principle. J Vibroeng. 2017;19(3):1494-1508.

[8] Yaguchi H, Sakuma S. A novel magnetic actuator capable of free movement on a magnetic substance. IEEE Trans Magn. 2015;51(11):4159-4162.

[9] Kato H, Marui E. Mechanical vibration. Japan: Corona Company; 1979. (In Japanese)